Spatiotemporal analyses illuminate the competitive advantage of a SARS-CoV-2 variant of concern over a variant of interest

Alexis Russell*[1], Collin O'Connor*[2,3], Erica Lasek-Nesselquist*[4,5], Jonathan Plitnick[1], John P. Kelly[6], Daryl M. Lamson[1], Kirsten St. George[1,5#]

*These authors contributed equally to this work.

[1] Laboratory of Viral Diseases, Wadsworth Center, New York State Department of Health, Albany, NY 12208, USA

[2] Division of Epidemiology, New York State Department of Health, Albany, NY 12242, USA

[3] Department of Geography, University at Buffalo, Buffalo, NY 14260

[4] Bioinformatics Core, Wadsworth Center, New York State Department of Health, Albany, NY 12208, USA

[5] Department of Biomedical Science, University at Albany, SUNY, Albany, NY 12208, USA

[6] Applied Genomic Technology Core, Wadsworth Center, New York State Department of Health, Albany, NY 12208, USA

[#] Corresponding Author, ORCID # 0000-0001-5168-763X

Short title: Analysis of the competitive advantage of SARS-CoV-2 variants

Abstract:

The emergence of novel SARS-CoV-2 variants in late 2020 and early 2021 raised alarm worldwide and prompted reassessment of the management, surveillance, and projected future of COVID-19. Mutations that confer competitive advantages by increasing transmissibility or immune evasion have been associated with the localized dominance of single variants. Thus, elucidating the evolutionary and epidemiological dynamics among novel variants is essential for understanding the trajectory of the COVID-19 pandemic. Here we show the interplay between B.1.1.7 (Alpha) and B.1.526 (Iota) in New York (NY) from December 2020 to April 2021 through phylogeographic analyses, space-time scan statistics, and cartographic visualization. Our results indicate that B.1.526 likely evolved in the Bronx in late 2020, providing opportunity for an initial foothold in the heavily interconnected New York City (NYC) region, as evidenced by numerous exportations to surrounding locations. In contrast, B.1.1.7 became dominant in regions of upstate NY where B.1.526 had limited presence, suggesting that B.1.1.7 was able to spread more efficiently in the absence of B.1.526. Clusters discovered from the spatial-time scan analysis supported the role of competition between B.1.526 and B.1.1.7 in NYC in March 2021 and the outsized presence of B.1.1.7 in upstate NY in April 2021. Although B.1.526 likely delayed the rise of B.1.1.7 in NYC, B.1.1.7 became the dominant variant in the Metro region by the end of the study period. These results reveal the advantages endemicity may grant to a variant (founder effect), despite the higher fitness of an introduced lineage. Our research highlights the dynamics of inter-variant competition at a time when B.1.617.2 (Delta) is overtaking B.1.1.7 as the dominant lineage worldwide. We believe our combined spatiotemporal methodologies can disentangle the complexities of shifting SARS-CoV-2 variant landscapes at a time when the evolution of variants with additional fitness advantages is impending.

Introduction:

The emergence of a novel SARS-CoV-2 variant B.1.1.7 (Alpha) in the United Kingdom (UK) in late 2020 raised alarm worldwide and prompted major reassessment of the management, surveillance, and projected future of COVID-19 (1,2). Evidence of increased transmissibility and potential immune evasion prompted the World Health Organization to designate B.1.1.7 a variant of concern (VOC) in December 2020 (3–6). Increased transmissibility of B.1.1.7 is likely due to several mutations, including N501Y which confers antibody evasion (7,8) and increases spike protein binding to the host cell (9), and del60-70 which enhances infectivity (10). The emergence of B.1.1.7 and additional novel SARS-CoV-2 variants with competitive advantages have resulted in localized dominance of single variants (11) and raised concern for increases in COVID-19 incidence (12).

Around the time B.1.1.7 emerged and became dominant in the UK, novel variant B.1.526 (Iota) arose from within New York State (NY) (13,14). The proportion of B.1.526 quickly increased in New York City (NYC) and led to a noticeable shift in lineage distribution during early 2021 (13,14). The World Health Organization designated B.1.526 as a variant of interest (VOI) due to its increase in prevalence coupled with mutations associated with immune evasion (15). Spike mutation E484K, which is present in approximately 45% of B.1.526 genomes sequenced in NY (GISAID.org) and is shared with the B.1.315 (Beta) and P.1 (Gamma) VOCs, is associated with reduced neutralization by monoclonal antibodies (16). Further, 29% of B.1.526 sequenced samples in NY possess the S477N spike mutation (GISAID.org), which likely evolved twice independently within the lineage (13). S477N is hypothesized to confer increased transmissibility due to its location at the ACE2 binding receptor in spike, which is

required for viral entry into the host cell. (17). Despite these concerns, an epidemiological assessment of B.1.526 in NYC from January through April 2021 found that the lineage did not cause more severe disease and was not associated with increased risk of reinfection or vaccine breakthrough (18).

Genomic surveillance of COVID-19 is a crucial tool to monitor and assess the physiological and epidemiological characteristics of SARS-CoV-2 variants as they emerge. In order to track the spread and impact of novel variants in NY, the New York State Department of Health (NYSDOH) significantly expanded its genomic surveillance program in December 2020, with the aim of sequencing a more representative subset of COVID-19 cases across the state. A robust genomic surveillance system allows for the assessment of changes in variant distribution over precise temporal and spatial scales. The co-circulation of B.1.526 and B.1.1.7 within NY in late 2020 and early 2021 offers a unique opportunity to compare variant transmission dynamics from a phylogeographic and spatial-epidemiological context. While phylogeographic analyses are routinely employed to infer the timing and source of SARS-CoV-2 introductions around the world (19–22), spatial statistics offer a complementary approach for examining COVID-19 incidence and the spatial spread of SARS-CoV-2 variants. Spatial statistics, including scan statistics for detecting clusters, are often employed in an epidemiological context to assess whether disease incidence is higher in one area than others (23). The discrete Poisson space-time scan statistic is a spatial statistical method that has been adopted to search for geographic areas with high incidence of COVID-19 (24,25). Similarly, the multinomial scan statistic is commonly used for the purposes of detecting geographic areas with unusually high distributions of specific

disease or event types. The multinomial scan statistic has been used to clarify categorical distributions in a variety of contexts, including the distribution of meningitis types (26), multiresistance phenotypes of Staphylococcus aureus (27), and methods of suicide (28). To the best of our knowledge, the use of multinomial scan statistic to quantitatively assess the categorical distribution of SARS-CoV-2 variants among total COVID-19 cases has not been reported. This study employs spatial scan statistics paired with phylogeographic analyses to describe the shifting SARS-CoV-2 variant landscape in NY from December 2020 to April 2021, particularly the inter-play between B.1.526 and B.1.1.7. We identify the sources of multiple introductions of B.1.1.7 and B.1.526 in NY and track their spatiotemporal spread relative to oneanother. As evidenced by the rapid dominance of the highly transmissible VOC Delta in many locations around the world in the summer of 2021 (GISAID.org), inter-variant competition will likely play a major role in the future public health response and epidemiology of COVID-19. Our findings elucidate the dynamics of competing SARS-CoV-2 variants at a time when the future variant landscape remains uncertain.

Results:

A total of 8,517 SARS-CoV-2 specimens sequenced by Wadsworth with collection dates between December 1, 2020 and April 30, 2021 were included in the study. Sequenced specimens equated to 0.6% of new COVID-19 cases in the study period. Among the included specimens, B.1.1.7 and B.1.526 constituted 1,107 (13%) and 904 (10.6%) of the samples, respectively. Formerly defined parent lineage B.1.526 and sublineages B.1.526.1, B.1.526.2, and B.1.526.3 constituted 98, 388, 415, and 2 samples, respectively. The average patient age for all samples

was 46.5 years, which decreased from 49.6 years in December to 39.5 years in April. Patient age and week of sample collection exhibited a negative association during the study (β=0.765, t= 16.31, p<0.0001). The mean age of sampled patients also differed significantly between variants (df=2, F=81.39, p<0.0001), where mean ages for B.1.1.7, B.1.526, and all other lineages were 39.3, 44.6, and 48.5 years, respectively.

The earliest B.1.1.7 samples sequenced by Wadsworth were collected on December 24, 2020 from a resident of Manhattan (Metro region) and an individual in Saratoga County (Capital region). B.1.1.7 remained relatively rare among all samples through the end of January. The Metro and Capital regions experienced the earliest increases in B.1.1.7, although the proportion of B.1.1.7 did not exceed 15% through February. The proportion of B.1.1.7 increased in March across all regions, most notably in the Western region where it constituted around 75% of all samples by the end of March and continued to rise through April. The Metro region experienced the most gradual increase in B.1.1.7, with the proportion not exceeding 40% until the end of April.

The earliest B.1.526 sample sequenced by Wadsworth was collected on December 9, 2020 from a patient in the Bronx (Metro region). The proportion of B.1.526 increased in the Metro region throughout December, reaching 10% of total samples by the end of the month. The proportion of B.1.526 in the Metro region approached 40% by the end of January, peaked at ~60% in mid-February to early March, and then plateaued around 50% through April. In contrast, B.1.526 was not consistently detected in the other regions until February, with increases after February in the Capital and Central regions, but the proportion generally remained under 40%. The Western region saw a minimal increase in B.1.526 after February, with the proportion

remaining under 15% through April. The combined proportion of all lineages other than B.1.1.7 and B.1.526 dropped below 20% in all NY regions by the end of April.

Maps of interpolated proportion of B.1.1.7 relative to all other lineages by ZCTA (Figure 1A) show a general trend of spread through the southern portion of NY in January, statewide distribution by February, diffuse increase in proportion in March, and a sustained high proportion throughout the state in April, with strong dominance in the Western region. In contrast, maps of interpolated proportion of B.1.526 shows more constricted initial spread focused around NYC and surrounding areas in January, with statewide distribution not achieved until March, and a moderate proportion sustained mostly within the Metro region, without notable increase in proportion from March to April (Figure 1B).

Maps of geographic mean centers of estimated B.1.1.7 and B.1.526 cases (Figure 2) show that shifts in the SARS-CoV-2 variant landscape had an impact on the spatial distribution of overall cases of COVID-19. The mean center of B.1.526 cases initially occurred near the NYC area, then gradually moved slightly northwest as B.1.526 expanded modestly into upstate regions. The mean center of B.1.1.7 cases was also in the NYC area at the beginning of the study period, then moved northwest during March and April to a much greater degree than for B.1.526 cases, indicating more substantial expansion of B.1.1.7 than B.1.526 outside of NYC. The mean centers of all COVID-19 cases showed a southeastern trajectory during December through March, but then exhibited a large northwestern shift in April, suggesting that the spread of B.1.1.7 in Upstate NY, especially within the Western region, resulted in a spatial shift of overall COVID-19 cases.

Retrospective multinomial space-time scan analysis indicated six statistically significant clusters with elevated relative risk (RR) of COVID-19 attributable to specific variants (Figure 3 and Table 1S). Two clusters of elevated RR of "Other" lineages were found in December, 2020 in the Metro/Capital regions as well as Long Island, reflecting the nearly non-existent risk for B.1.1.7 and B.1.526. Of note, these clusters are likely to be limited in spatial extent due to setting the maximum cluster size to 10% of the population-at-risk, as the presence of B.1.1.7 and B.1.526 were also nearly non-existent statewide in December (Figure 1). Three clusters of elevated RR of multiple combinations of B.1.1.7, B.1.526 parent lineage, B.1.526.1, and B.1.526.2 were found in March, 2021 in the NYC/Long Island region. The sixth cluster exhibited an elevated RR of greater than 7.0 for B.1.1.7, with a radius of 114.38 km centered in the Finger Lakes area (Western and Central regions) during April. Additionally, the presence of clusters of B.1.1.7 and B.1.526 in March and April coincide with a general statewide decrease in incidence of COVID-19 (Figure 3).

The final B.1.526 dataset for phylogenetic reconstruction contained 980 genomes from all regions of NY and various domestic locations (Bronx: 222, Hudson Valley: 128, Brooklyn: 39, Long Island: 78, Manhattan: 49, Queens: 81, Staten Island: 12, Upstate NY: 81, Domestic: 290). The final B.1.1.7 dataset contained 1,195 genomes from the NYC region (181), Finger Lakes (239), Hudson Valley (78), Long Island (130), Western NY and the Southern Tier (Southwestern NY: 56), Capital District, Mohawk Valley, Central NY and the North Country (Northern NY: 149), as well as other states (Domestic: 362). Results from the phylogeographic analysis indicated that B.1.526 emerged within the Bronx near the end of 2020, and that this location was the major source of spread to other regions of NY and US (Domestic) in the

ensuing months (Figure 4A). Although sampling biases could have influenced the number of introductions assigned to the Bronx, the Domestic category had greater representation in the dataset but led to substantially fewer introductions (Table S2). Specifically, Domestic genomes represented 29.5% of the dataset but this location was responsible for only 6.7% of all B.1.526 introductions, while the Bronx represented 22.7% of the dataset and led to 63.8% of all introductions (Table S2). Excluding the Bronx, B.1.526 transmission between boroughs and from these boroughs to other NY or Domestic locations was relatively infrequent. Further, introductions were mostly uni-directional, with only 9% of the B.1.526 cases sequenced from the Bronx due to re-introductions. This indicates the spread of B.1.526 in the Bronx was overwhelmingly attributable to transmission within the Bronx itself and contrasts the trends for other NY and Domestic locations, which showed more limited sustained transmission of B.1.526 as a function of the ratio of number of introductions to sample size.

Multiple domestic introductions contributed to the initial presence of B.1.1.7 in NY (29), with transmission occurring most frequently to the Finger Lakes and Northern NY (Figure 4B). The Finger Lakes and Northern NY were well-represented in the dataset (20% and 12% of the data, respectively) but contributed substantially less to the distribution of B.1.1.7 (accounting for 7% and 6% of the total number of introductions, respectively) than Domestic sites, which represented 20% of the data and were responsible for the majority of introductions (~39%, Table S3). Exchange between NYC and Long Island and NYC and the Hudson Valley was also frequent, but transmission from these regions to Northern NY, Southwestern NY, and the Finger Lakes was substantially more limited (Figure 4B, Table 3), possibly reflecting the effects of interconnectivity in a metropolitan area dominated by commuter activity. The Finger Lakes

showed the lowest proportion of sequenced cases due to introductions but the largest sample size in NY, suggesting more sustained transmission of B.1.1.7 within this region. The topologies of the B.1.526 and B.1.1.7 phylogenetic trees highlight differences in transmission patterns as well. Introductions of B.1.526 often represent single events not associated with additional transmission (except for some introductions from the Bronx), which led to B.1.526 genomes from various locations being distributed broadly throughout the tree. In contrast, introductions of B.1.1.7 often led to large regional clusters, such as those in the Finger Lakes from Domestic sources, producing a patchier distribution of genomes from the same region.

Discussion:

The repeated emergence of novel variants of SARS-CoV-2 has largely defined the COVID-19 pandemic response in 2021. As vaccination rates, prior exposure levels, and behavioral public health measures continuously change, so too does the strength of selection (30). Given that selective pressures likely vary across regions, including between and within states, it follows that the emergence and spread of SARS-CoV-2 variants are also regionally dynamic. We combine spatial statistical, phylogeographic, and cartographic visualization techniques to examine the spatiotemporal dynamics of the VOC B.1.1.7 (Alpha) and the VOI B.1.526 (Iota) within NY from December 2020 through April 2021. Our study period captures a time of substantial fluctuations in statewide COVID-19 incidence, with a major peak in late December and early January followed by decline through February, and then a smaller peak in late March and early April followed by a decline through April. The peak incidence in late 2020 and early 2021 represents the second major wave of COVID-19 cases in NYC, and the first

major wave for much of the rest of the state. Our study period also spans the launch of NY's vaccination campaign in January 2021 and subsequent rise in immunization rates.

The concurrent spread of B.1.1.7 and B.1.526 offers a unique opportunity to compare the dynamics of two competing variants of SARS-CoV-2 within a population. Shortly after its appearance in the Bronx in late 2020, B.1.526 quickly became the most common lineage in NYC and the surrounding region by mid-February. The rapid dominance of B.1.526 within NYC is corroborated by time-calibrated phylogeny (Figure 4A), which depicts widespread initial transmission within the Bronx, periodic introductions to neighboring boroughs, and later introductions to the greater Metro region and other states, with few introductions leading to sustained transmission outside the Bronx. The spread of B.1.526 appears to have been spatially limited by the repeated introduction and apparent transmission advantage of B.1.1.7 outside of NYC. Regions of NY where B.1.526 had not yet established experienced rapid dominance of B.1.1.7 during March and April. This trend is most clearly seen in the near complete displacement of all other lineages by B.1.1.7 in Western NY (Supplemental Figure 1A), resulting in a large cluster of elevated RR for B.1.1.7 cases in the Finger Lakes region during April (Figure 3). Phylogeographic analysis provides support for the sustained transmission of B.1.1.7 in the Finger Lakes, evidenced by the large regional clusters resolved in the tree. The multinomial spatial scan detected three unique clusters in March 2021, all with increased RR for B.1.1.7 and B.1.526. The values for RR within each NYC cluster details a distinct pattern: clusters centered within the Bronx, Brooklyn, and Manhattan had higher RR for

B.1.526, while the cluster centered in east Queens and Long Island had a higher RR for B.1.1.7 (Table S1). Over the months following B.1.526's initial advantage in NYC, B.1.1.7 trends towards become the majority variant in the Metro region. Despite the presence of both B.1.1.7 and B.1.526 in the Metro region in the early months of 2021, phylogeographic analyses indicated that the parental lineage of B.1.526 was circulating in the Bronx by August 2020, with more frequent transmission to Manhattan than Long Island. While B.1.1.7 was circulating in Long Island by mid-October 2020, almost all B.1.526 introductions to this region occurred in 2021. Thus, there are important distinctions between the spread of B.1.1.7 and B.1.526 even within a geographically proximal area. The delayed dominance of B.1.1.7 in the Bronx compared to Long Island and Queens suggests that B.1.526 was more difficult to displace than other lineages circulating in these areas. The number of B.1.1.7 introductions into NYC was greater than into the Finger Lakes, but sustained transmission was less prevalent, providing further evidence that widespread circulation of B.1.526 in NYC stunted the initial spread of B.1.1.7 in this area. Maps of the geographic mean centers of the estimated number of COVID-19 cases attributable to each variant capture the rapid spread of B.1.1.7 out of NYC, as well as the relative inability of B.1.526 to claim a foothold outside of the Metro region. The northwesterly shift in the trajectory of overall COVID-19 cases in April indicates that the expansion of B.1.1.7, in particular clustering in Western NY, had a measurable influence on the spatial spread of COVID-19 cases overall.

There are several limitations of our study which primarily reflect the inherent limitations of our genomic surveillance program. A degree of selection bias exists within our dataset given that specimens were screened by cycle threshold value and were submitted by a selected group

of clinical and commercial labs that cannot perfectly represent all COVID-19 cases in NY. We were unable to assess the demographic and clinical representativeness of our dataset because these data were not available to us for many specimens. Additionally, the number of specimens sequenced varied over the space and time of the study period, which created small sample sizes within many ZCTA-months. This limitation extended to the multinomial scan statistic, which was run with estimated values for COVID-19 cases attributable to B.1.1.7 and B.1.526, giving all ZCTAs with samples equal weight. However, the spatial scan assesses data according to their proximity to each other. In this context, ZCTAs are analyzed together rather than individually, which has the potential to reduce bias. Another consequence of our limited sampling was that our data exhibited zero samples from many ZCTAs for each month. We addressed this by using IDW interpolation of the proportion of B.1.1.7 and B.1.526 sequenced samples at the ZCTA-month level to visualize general patterns of variant proportions over geography. Phylogeographic analyses were hampered by similar limitations: uneven sampling among regions and the lack of global representation in our datasets could lead to incorrect trait assignments. Smaller sample sizes for some regions might have caused an underestimation of their contributions to variant transmission in NY while larger sample sizes might have inflated the number of introductions assigned. However, we believe the results presented here largely capture the transmission dynamics of B.1.526 and B.1.1.7 within NY, as smaller sample sizes were consistent with lower incidence, while larger sample sizes did not always correspond to regions with outsized contributions to the spread of either variant.

Our results are in general agreement with those of Petrone et al. 2021, who showed that

B.1.1.7 had a higher reproductive value and was able to spread faster than B.1.526 in Connecticut, where both variants were introduced a similar number of times. The reproductive value for B.1.1.7 in NYC was also higher than B.1.526 but the data were noisier, which supports our conclusions that the clear advantage B.1.1.7 showed in Western NY and the Finger Lakes was obfuscated in NYC by the initial dominating presence of B.1.526.

Our phylogeographic and spatiotemporal analyses offer a methodology for evaluating the relative transmissibility and competitive advantages of co-circulating SARS-CoV-2 variants. We demonstrate that the emergence of VOI B.1.526 slowed the rise of VOC B.1.1.7 within NYC, while B.1.1.7 simultaneously became the majority variant in parts of NY devoid of B.1.526. In this way, our study describes important dynamic interactions between variants with unequal transmissibility and is potentially generalizable to interactions between any known variant and the highly transmissible B.1.617.2 (Delta) variant and other variants to come. As B.1.617.2 continues to change the variant landscape on local and global levels, understanding its dynamic interactions with other variants is increasingly important in the management of COVID-19.

Methods:

Sample acquisition and RNA extraction

The NYSDOH Wadsworth Center coordinated with over 30 clinical laboratories throughout NY who routinely submitted respiratory swabs positive for SARS-CoV-2 for whole genome sequencing. Specimens were required to have a real-time cycle threshold value less than 30. Nucleic acid extraction was performed on a Roche MagNAPure 96 with the Viral NA Small Volume Kit (Roche, Indianapolis, IN) with 100µL sample input and 100µL eluate.

305 Sequencing and bioinformatics processing

306 Extracted RNA was processed for whole genome sequencing with a modified ARTIC
307 protocol (artic.network/ncov-2019) in the Applied Genomics Technology Core at the Wadsworth
308 Center as previously described (29); supplementary information). Illumina libraries were
309 processed with ARTIC nextflow pipelines
310 (github.com/connorlab/ncov2019/articnf/tree/illumine, last updated April 2020) as previously
311 described (Alpert et al., 2021; supplementary information)

312 Sample inclusion criteria

313 Specimens with collection dates between December 1, 2020 and April 30, 2021 were
314 included. Specimens that were sequenced as a result of pre-screening for specific mutations or
315 clinical/epidemiological criteria were removed from the analysis. In the case of duplicate
316 specimens from the same patient, the earliest collected specimen was included, and all other
317 specimens excluded from the analysis. Only specimens with ZIP code of patient address
318 available were included.

319 COVID incidence calculation

320 Monthly COVID case counts by ZIP code were obtained from
321 https://gibhub.com/nychealth/coronavirus-data for NYC, and from the NYSDOH Communicable
322 Disease Electronic Surveillance System for the remainder of NY. Reports with case status of
323 'confirmed' or 'probable' were included in the case count. Cases were assigned month based on
324 date of diagnosis. All ZIP code data was converted to ZIP code tabulation area (ZCTA).
325 Incidence was calculated using ZCTA-level population data from the 2019 1-year American
326 Community Survey estimates.

Retrospective multinomial space-time scan statistic

We utilize the retrospective multinomial space-time scan statistic in SaTScan version 9.6, using the non-ordinal method (26,31). Estimated SARS-CoV-2 variant data used in the multinomial scan statistic were calculated for each ZCTA-month aggregation by multiplying the proportion of either B.1.1.7, B.1.526, or "Other" variants in our sample by the total number of COVID-19 cases.

Maximum spatial and temporal cluster size parameters were set a priori for 10% of the population at risk (24) and one month, respectively. Space-time cluster detection in SaTScan has a noted limitation where the size of clusters cannot change over time (32,33). Given that our data is aggregated to the temporal unit of months (December 2020 – April 2021), setting the maximum temporal cluster size parameter to one month allows clusters to change their shape from month to month by being designated as "new" clusters. A further description of settings for the retrospective multinomial space-time scan statistic can be found in the supplemental materials.

Inverse-distance weighted interpolation and spatial average of SARS-CoV-2 genome sequencing

We employed inverse-distance weighted (IDW) interpolation to better visualize how the proportion of COVID-19 cases attributable to each SARS-CoV-2 variant spatiotemporally varies in NY (34). The percentage of COVID-19 cases attributable to each variant in a ZCTA was assigned each ZCTA's corresponding centroid for the IDW calculation. IDW interpolation generated a continuous surface of values representing the percentage of total COVID-19 cases attributed to B.1.1.7 and B.1.526, which were then averaged over each ZCTA geometry.

The estimated percentage of each SARS-CoV-2 variant generated from IDW interpolation was then multiplied by the total number of COVID-19 cases for each ZCTA and month of our study period to estimate the total number of COVID-19 cases attributable to each variant. Estimated numbers of variant cases were then used to generate geographic mean centers for each month of the study period for visualization (35). Methods for geographic mean center calculation can be found in the supplemental materials.

Phylogeographic analyses

All B.1.526 genomes from the United States (US) and associated metadata (excluding NY sequences) were downloaded from GISAID (GISAID.org) and randomly subsampled to approximately equal depth as the heaviest sampled NY region in our dataset, with the number of genomes from each state sampled proportionally to their overall frequency in the US. The final dataset included B.1.526 genomes from MA, NJ, PA, CT, CA, FL, MD, MI, MN, and NC, aggregated as “Domestic”, genomes from the five boroughs of NYC (Bronx, Brooklyn, Queens, Staten Island, Manhattan), Long Island, and the Hudson Valley and those from Western NY, the Finger Lakes, the Capital District, and Central NY regions aggregated as “Upstate”. Genomes were aligned in mafft v7.475 (36) with problematic sites masked according to (https://github.com/W-L/ProblematicSites_SARS-CoV-2). A maximum likelihood phylogeny was generated in IQTree v1.6.12 (37) with 1000 ultrafast bootstrap replicates (38) and timecalibrated in TreeTime v0.7.6 (39). This tree served as the fixed tree for ancestral state reconstruction in Beast v2.6.2 (40) to infer timing and source of B.1.526 introductions within the state of NY. The Bayesian analysis was allowed to run for > 4 million generations and monitored in Tracer until the effective sample size of all parameters >= 200 and the MCMC chain appeared to reach stationarity.

A B.1.1.7 phylogeographic analysis was conducted in the same manner with the states inferred for a fixed topology over 6 million generations in BEAST2 under an exponential coalescent model until all ESS reach >= 200. The final dataset included B.1.1.7 genomes from MA, PA, CT, NJ, CA, and FL grouped together as "Domestic", the NYC, Long Island, MidHudson and Finger Lakes regions of NY, "Southwest NY" composed of the Southern Tier and Western regions of NY, and "Northern NY" comprised of the Capital District, Mohawk Valley,
Central NY, and the North Country.

Maximum clade credibility trees for B.1.526 and B.1.1.7 were generated in TreeAnnotator v.2.6.2 (40) with a 10% burn-in. The number of introductions between locations was summarized by Baltic (https://github.com/evogytis/baltic) by adopting the exploded tree script for Python 3. Only introductions with a posterior probability of 0.7 >= were considered. Trees were visualized in FigTree v1.5.5 (http://tree.bio.ed.ac.uk/software/figtree/) and ggtree (41) for R v4.1.0 (http://www.R-project.org) (see supplementary information for additional details).

Figure captions:

Figure 1: Inverse distance weighted interpolations of A) percent of B.1.1.7 and B) percent of B.1.526 relative to all other lineages by ZIP code tabulation area.

Figure 2: Geographically weighted mean centers of total COVID-19 cases and estimated COVID-19 cases attributable to B.1.526 and B.1.1.7, December 2020 through April 2021.

Cluster centroids refer to the results of the multinomial space-time scan analysis (Figure 3).

Figure 3: SARS-CoV-2 variant clusters identified from retrospective multinomial space-time scan analysis and COVID-19 incidence by ZIP code tabulation area, December 2020 through April 2021.

Figure 4:

A) Time-calibrated phylogeny of SARS-CoV-2 variant B.1.526. Left panel represents a maximum likelihood phylogeny of 908 genomes from New York and other states generated in IQ-tree with timescale inferred by TreeTime and ancestral state reconstruction performed in BEAST. Faceted panels indicate the source of B.1.526 introductions into different region of New York or other states (Domestic). Only introductions supported by an ancestral state probability of >= 0.7 are shown. Right panel shows locations sampled and sample sizes.

B) Time-calibrated phylogeny of SARS-CoV-2 variant B.1.1.7. Left panel represents a maximum likelihood phylogeny of 1,195 genomes from New York and other states generated in IQ-Tree with timescale inferred by TreeTime and ancestral state reconstruction performed in BEAST. The tree was rooted with a P.1 genomes (not shown). Faceted panels indicate the source of B.1.1.7 introductions into different regions of New York and to other states (Domestic). Only introductions supported by an ancestral state probability of >= 0.7 are shown. Right panel shows locations sampled and sample sizes.

IRB Approval

This work was approved by the New York State Department of Health Institutional Review Board, under study numbers 02-054 and 07-022.

Acknowledgements

The authors gratefully acknowledge the Advanced Genomic Technologies Core of the Wadsworth Center where all next generation sequencing was performed. We also graciously thank the New York State clinical laboratories that submitted SARS-CoV-2 positive specimens to Wadsworth for sequence analysis, all originating and submitting laboratories for their SARS-CoV-2 sequence contributions to the GISAID database, Wadsworth Center's Virology Laboratory for initial processing of specimens and the Bioinformatics Core for sequence processing and analysis.

References:

1. Grubaugh ND, Hodcroft EB, Fauver JR, Phelan AL, Cevik M. Public health actions to control new SARS-CoV-2 variants. Cell. 2021 Mar;184(5):1127–32.

2. Lauring AS, Hodcroft EB. Genetic Variants of SARS-CoV-2—What Do They Mean? JAMA. 2021 Feb 9;325(6):529.

3. Frampton D, Rampling T, Cross A, Bailey H, Heaney J, Byott M, et al. Genomic characteristics and clinical effect of the emergent SARS-CoV-2 B.1.1.7 lineage in London, UK: a whole-genome sequencing and hospital-based cohort study. The Lancet Infectious Diseases. 2021 Apr;S1473309921001705.

4. Haynes WA, Kamath K, Lucas C, Shon J, Iwasaki A. Impact of B.1.1.7 variant mutations on antibody recognition of linear SARS-CoV-2 epitopes [Internet]. Infectious Diseases (except HIV/AIDS); 2021 Jan [cited 2021 Jun 18]. Available from:

http://medrxiv.org/lookup/doi/10.1101/2021.01.06.20248960

5. Kidd M, Richter A, Best A, Cumley N, Mirza J, Percival B, et al. S-Variant SARS-CoV-2 Lineage B1.1.7 Is Associated With Significantly Higher Viral Load in Samples Tested by TaqPath Polymerase Chain Reaction. The Journal of Infectious Diseases. 2021 May 28;223(10):1666–70.

6. Planas D, Bruel T, Grzelak L, Guivel-Benhassine F, Staropoli I, Porrot F, et al. Sensitivity of infectious SARS-CoV-2 B.1.1.7 and B.1.351 variants to neutralizing antibodies. Nat Med. 2021 May;27(5):917–24.

7. Peters MH, Bastidas O, Kokron DS, Henze CE. Transformations, Lineage Comparisons, and Analysis of Down to Up Protomer States of Variants of the SARS-CoV-2 Prefusion Spike Protein Including the UK Variant B.1.1.7 [Internet]. Biophysics; 2021 Feb [cited 2021 Jun 18]. Available from: http://biorxiv.org/lookup/doi/10.1101/2021.02.09.430519

8. Wibmer CK, Ayres F, Hermanus T, Madzivhandila M, Kgagudi P, Oosthuysen B, et al. SARS-CoV-2 501Y.V2 escapes neutralization by South African COVID-19 donor plasma. Nat Med. 2021 Apr;27(4):622–5.

9. Tian F, Tong B, Sun L, Shi S, Zheng B, Wang Z, et al. Mutation N501Y in RBD of Spike Protein Strengthens the Interaction between COVID-19 and its Receptor ACE2 [Internet]. Biophysics; 2021 Feb [cited 2021 Jun 18]. Available from: http://biorxiv.org/lookup/doi/10.1101/2021.02.14.431117

10. Meng B, Kemp SA, Papa G, Datir R, Ferreira IATM, Marelli S, et al. Recurrent emergence of SARS-CoV-2 spike deletion H69/V70 and its role in the variant of concern lineage B.1.1.7. Cell Reports. 2021 Jun;109292.

11. Volz E, Mishra S, Chand M, Barrett JC, Johnson R, Geidelberg L, et al. Transmission of SARS-CoV-2 Lineage B.1.1.7 in England: Insights from linking epidemiological and genetic data [Internet]. Infectious Diseases (except HIV/AIDS); 2021 Jan [cited 2021 Jan 12]. Available from: http://medrxiv.org/lookup/doi/10.1101/2020.12.30.20249034

12. Tegally H, Wilkinson E, Giovanetti M, Iranzadeh A, Fonseca V, Giandhari J, et al. Emergence and rapid spread of a new severe acute respiratory syndrome-related coronavirus 2 (SARS-CoV-2) lineage with multiple spike mutations in South Africa [Internet]. Epidemiology; 2020 Dec [cited 2021 Jun 15]. Available from: http://medrxiv.org/lookup/doi/10.1101/2020.12.21.20248640

13. Lasek-Nesselquist E, Lapierre P, Schneider E, George KSt, Pata J. The localized rise of a B.1.526 SARS-CoV-2 variant containing an E484K mutation in New York State [Internet]. Epidemiology; 2021 Mar [cited 2021 Jul 26]. Available from: http://medrxiv.org/lookup/doi/10.1101/2021.02.26.21251868

14. West AP, Wertheim JO, Wang JC, Vasylyeva TI, Havens JL, Chowdhury MA, et al.

Detection and characterization of the SARS-CoV-2 lineage B.1.526 in New York [Internet]. Bioinformatics; 2021 Feb [cited 2021 Jun 18]. Available from: http://biorxiv.org/lookup/doi/10.1101/2021.02.14.431043

15. World Health Organization. Epidemiological update: Variants of SARS-CoV-2 in the Americas. [Internet]. 2021 Mar. Available from: https://iris.paho.org/handle/10665.2/53382

16. Harvey WT, Carabelli AM, Jackson B, Gupta RK, Thomson EC, Harrison EM, et al. SARS-CoV-2 variants, spike mutations and immune escape. Nat Rev Microbiol. 2021 Jul;19(7):409–24.

17. Hodcroft EB, Zuber M, Nadeau S, Crawford KHD, Bloom JD, Veesler D, et al. Emergence and spread of a SARS-CoV-2 variant through Europe in the summer of 2020. medRxiv. 2020 Jan 1;2020.10.25.20219063.

18. Thompson CN, Hughes S, Ngai S, Baumbartner J, Wang JC, McGibbon E, et al. Rapid Emergence and Epidemiologic Characteristics of the SARS-CoV-2 B.1.526 Variant - New York City, New York, January 1 - April 5, 2021. MMWR. 2021 May 14;70(19):712–6.

19. Gonzalez-Reiche AS, Hernandez MM, Sullivan MJ, Ciferri B, Alshammary H, Obla A, et al. Introductions and early spread of SARS-CoV-2 in the New York City area. Science. 2020 Jul 17;369(6501):297.

20. Maurano MT, Ramaswami S, Zappile P, Dimartino D, Boytard L, Ribeiro-dos-Santos AM, et al. Sequencing identifies multiple early introductions of SARS-CoV-2 to the New York City Region. medRxiv. 2020 Jan 1;2020.04.15.20064931.

21. Rambaut, Andrew. Phylodynamic Analysis | 176 genomes [Internet]. https://virological.org. 2020 [cited 2020 Nov 17]. Available from: https://virological.org/t/phylodynamic-analysis176-genomes-6-mar-2020/356

22. Worobey M, Pekar J, Larsen BB, Nelson MI, Hill V, Joy JB, et al. The emergence of SARS-CoV-2 in Europe and North America. Science. 2020 Oct 30;370(6516):564.

23. Kulldorff M, Nagarwalla N. Spatial disease clusters: Detection and inference. Statist Med. 1995 Apr 30;14(8):799–810.

24. Desjardins MR, Hohl A, Delmelle EM. Rapid surveillance of COVID-19 in the United States using a prospective space-time scan statistic: Detecting and evaluating emerging clusters. Applied Geography. 2020 May;118:102202.

25. Rosillo N, Del-Águila-Mejía J, Rojas-Benedicto A, Guerrero-Vadillo M, Peñuelas M, Mazagatos C, et al. Real time surveillance of COVID-19 space and time clusters during the summer 2020 in Spain. BMC Public Health. 2021 Dec;21(1):961.

26. Jung I, Kulldorff M, Richard OJ. A spatial scan statistic for multinomial data. Statist Med. 2010 Aug 15;29(18):1910–8.

27. Stelling J, Read JS, Peters R, Clark A, Bokhari M, O'Brien TF. Staphylococcus aureus antimicrobial susceptibility trends and cluster detection in Vermont: 2012-2018. Expert Review of Anti-infective Therapy. 2021 Jun 3;19(6):777–85.

28. Ngamini Ngui A, Apparicio P, Moltchanova E, Vasiliadis H-M. Spatial analysis of suicide mortality in Québec: Spatial clustering and area factor correlates. Psychiatry Research. 2014 Dec;220(1–2):20–30.

29. Alpert T, Brito AF, Lasek-Nesselquist E, Rothman J, Valesano AL, MacKay MJ, et al. Early introductions and transmission of SARS-CoV-2 variant B.1.1.7 in the United States. Cell. 2021 May 13;184(10):2595-2604.e13.

30. Neher R. The virus is under increasing selection pressure [Internet]. 2021 [cited 2021 Aug 10]. Available from: https://www.mpg.de/16371358/coronavirus-variants

31. Kulldorff M. Software for the spatial and space-time scan statistics [Internet]. Information Mangement Services, Inc.; 2018. Available from: http://www.satscan.org/

32. Iyengar VS. Space-time clusters with flexible shapes. MMWR Suppl. 2005 Aug 26;54:71–6.

33. Takahashi K, Kulldorff M, Tango T, Yih K. A flexibly shaped space-time scan statistic for disease outbreak detection and monitoring. Int J Health Geogr. 2008;7(1):14.

34. Shepard D. A two-dimensional interpolation function for irregularly-spaced data. In: Proceedings of the 1968 23rd ACM national conference on - [Internet]. Not Known: ACM Press; 1968 [cited 2021 Jun 8]. p. 517–24. Available from: http://portal.acm.org/citation.cfm?doid=800186.810616

35. Rogerson PA, Plane DA. Geographical Analysis of Population: With Applications to Planning and Business. Internat.ed. John Wiley and Sons Ltd; 1994. 416 p.

36. Katoh K, Standley DM. MAFFT multiple sequence alignment software version 7: improvements in performance and usability. Mol Biol Evol. 2013 Apr;30(4):772–80.

37. Nguyen L-T, Schmidt HA, von Haeseler A, Minh BQ. IQ-TREE: A Fast and Effective Stochastic Algorithm for Estimating Maximum-Likelihood Phylogenies. Mol Biol Evol. 2015 Jan 1;32(1):268–74.

38. Minh BQ, Nguyen MAT, von Haeseler A. Ultrafast Approximation for Phylogenetic Bootstrap. Molecular Biology and Evolution. 2013 Feb 15;30(5):1188–95.

39. Sagulenko P, Puller V, Neher RA. TreeTime: Maximum-likelihood phylodynamic analysis. Virus Evolution [Internet]. 2018 Jan 8 [cited 2020 Jul 15];4(vex042). Available from: https://doi.org/10.1093/ve/vex042

551 40. Bouckaert R, Vaughan TG, Barido-Sottani J, Duchêne S, Fourment M, Gavryushkina A, et
552 al. BEAST 2.5: An advanced software platform for Bayesian evolutionary analysis. PLOS
553 Computational Biology. 2019 Apr 8;15(4):e1006650.

552 41. Yu G, Smith DK, Zhu H, Guan Y, Lam TT-Y. ggtree: an r package for visualization and
553 annotation of phylogenetic trees with their covariates and other associated data. Methods in 554 Ecology and Evolution. 2017 Jan 1;8(1):28–36.

555

Figure 1A

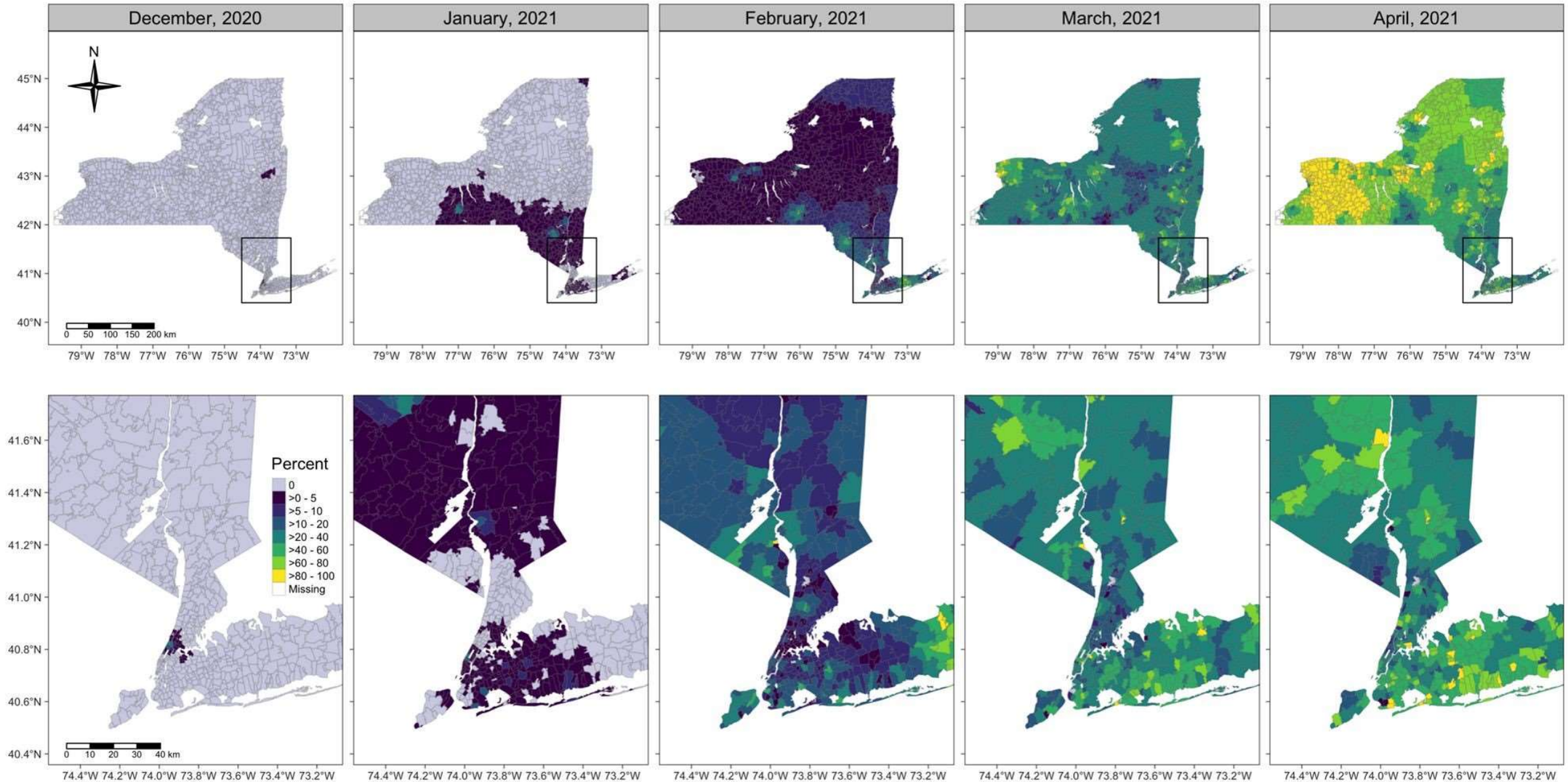
December, 2020
January, 2021
February, 2021
March, 2021
April, 2021
N
45°N
44°N
43°N
42°N
41°N
40°N
0 50 100 150 200 km
79°W 78°W 77°W 76°W 75°W 74°W 73°W
41.6°N
41.4°N
41.2°N
41.0°N
40.8°N
40.6°N
40.4°N
0 10 20 30 40 km
74.4°W 74.2°W 74.0°W 73.8°W 73.6°W 73.4°W 73.2°W
Percent
0
>0 - 5
>5 - 10
>10 - 20
>20 - 40
>40 - 60
>60 - 80
>80 - 100
Missing

Figure 1B

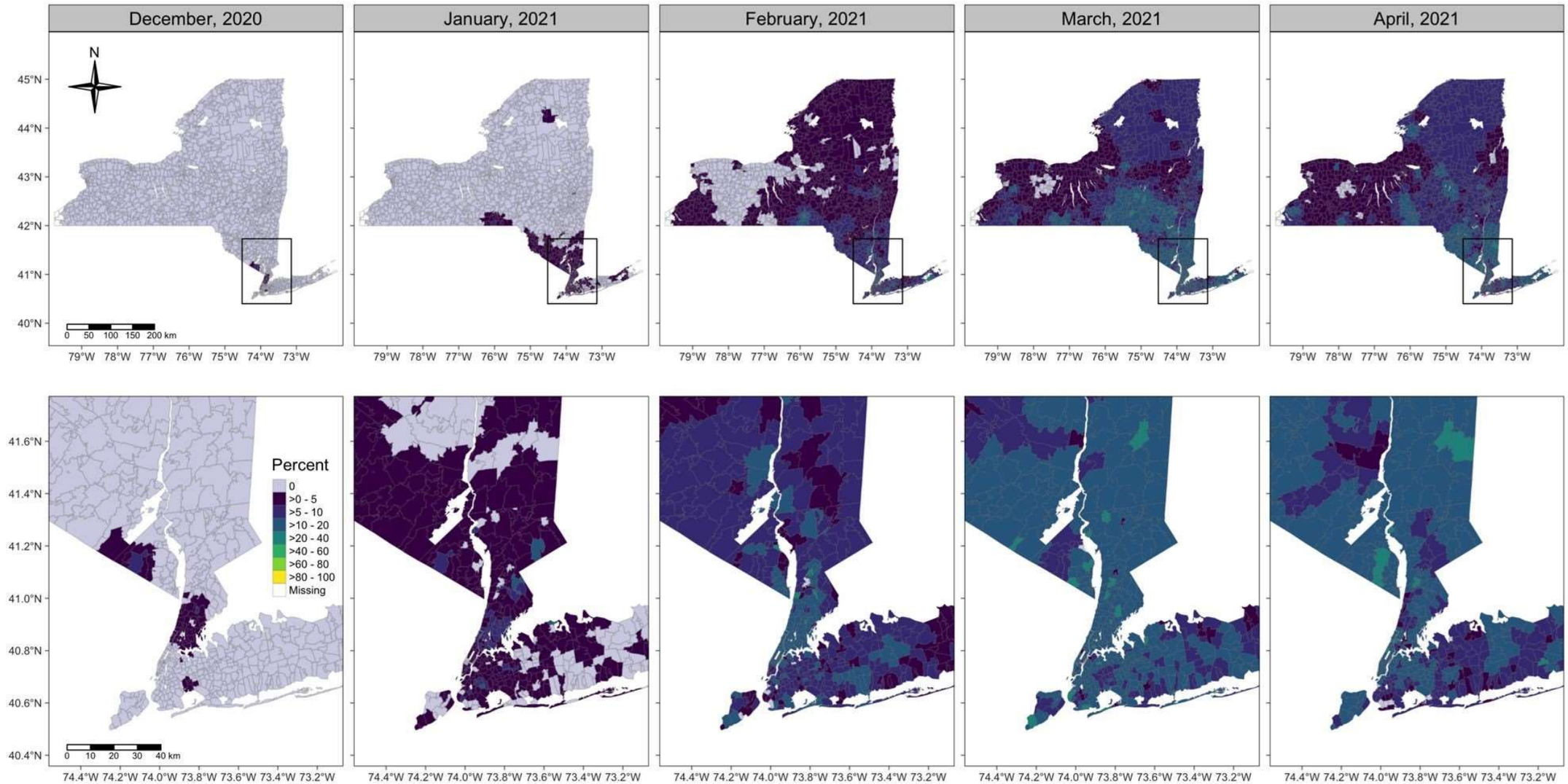
December, 2020
January, 2021
February, 2021
March, 2021
April, 2021
N
45°N
44°N
43°N
42°N
41°N
40°N
0 50 100 150 200 km
79°W 78°W 77°W 76°W 75°W 74°W 73°W
41.6°N
41.4°N
41.2°N
41.0°N
40.8°N
40.6°N
40.4°N
0 10 20 30 40 km
74.4°W 74.2°W 74.0°W 73.8°W 73.6°W 73.4°W 73.2°W
Percent
0
>0 - 5
>5 - 10
>10 - 20
>20 - 40
>40 - 60
>60 - 80
>80 - 100
Missing

Figure 2

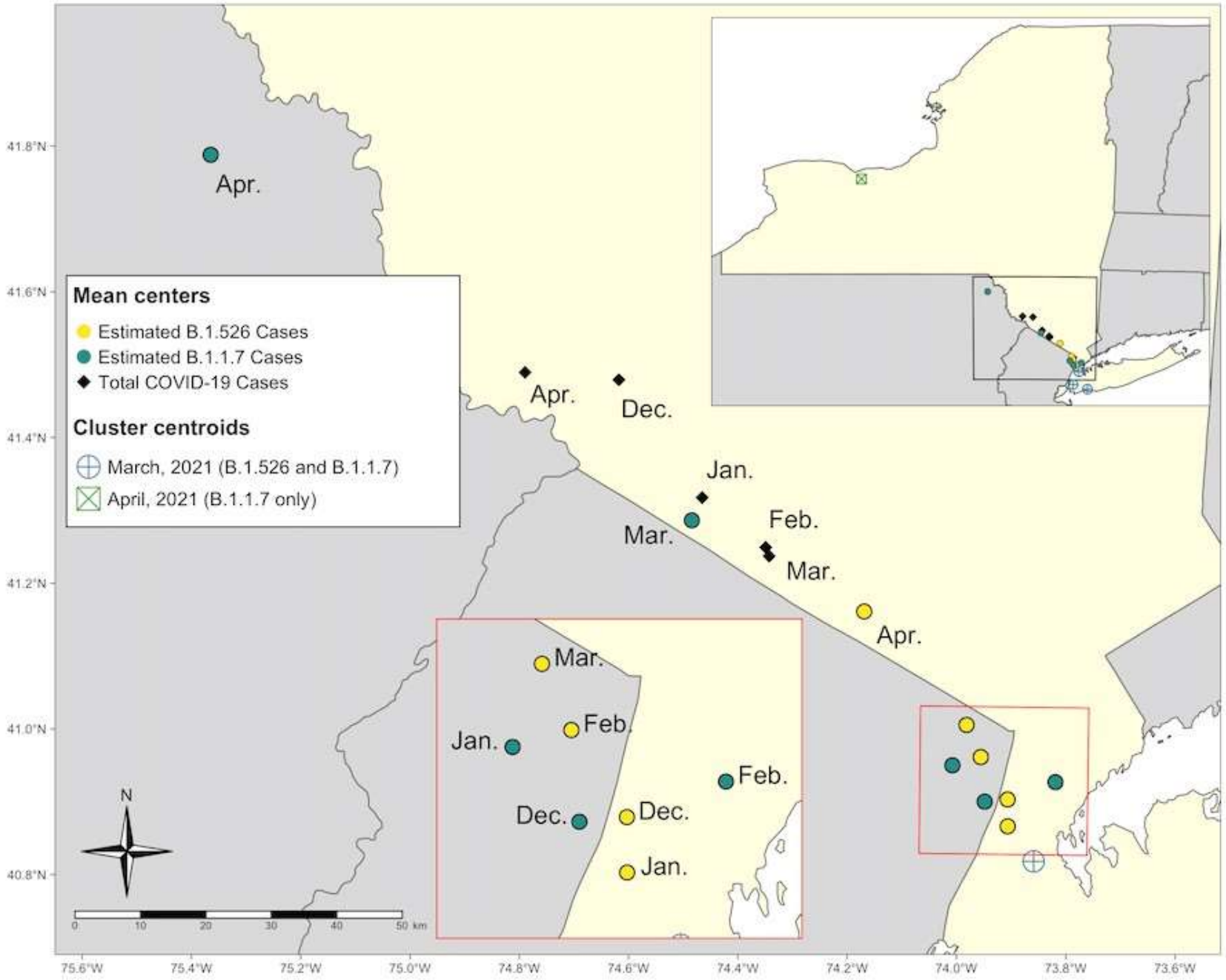
Mean centers
Estimated B.1.526 Cases
Estimated B.1.1.7 Cases
Total COVID-19 Cases
Cluster centroids
March, 2021 (B.1.526 and B.1.1.7)
April, 2021 (B.1.1.7 only)
Apr.
Apr.
Dec.
Jan.
Feb.
Mar.
Mar.
Apr.
Mar.
Feb.
Jan.
Feb.
Dec.
Dec.
Jan.
N
0
10
20
30
40
50 km
41.8°N
41.6°N
41.4°N
41.2°N
41.0°N
40.8°N
75.6°W
75.4°W
75.2°W
75.0°W
74.8°W
74.6°W
74.4°W
74.2°W
74.0°W
73.8°W
73.6°W

Figure 3

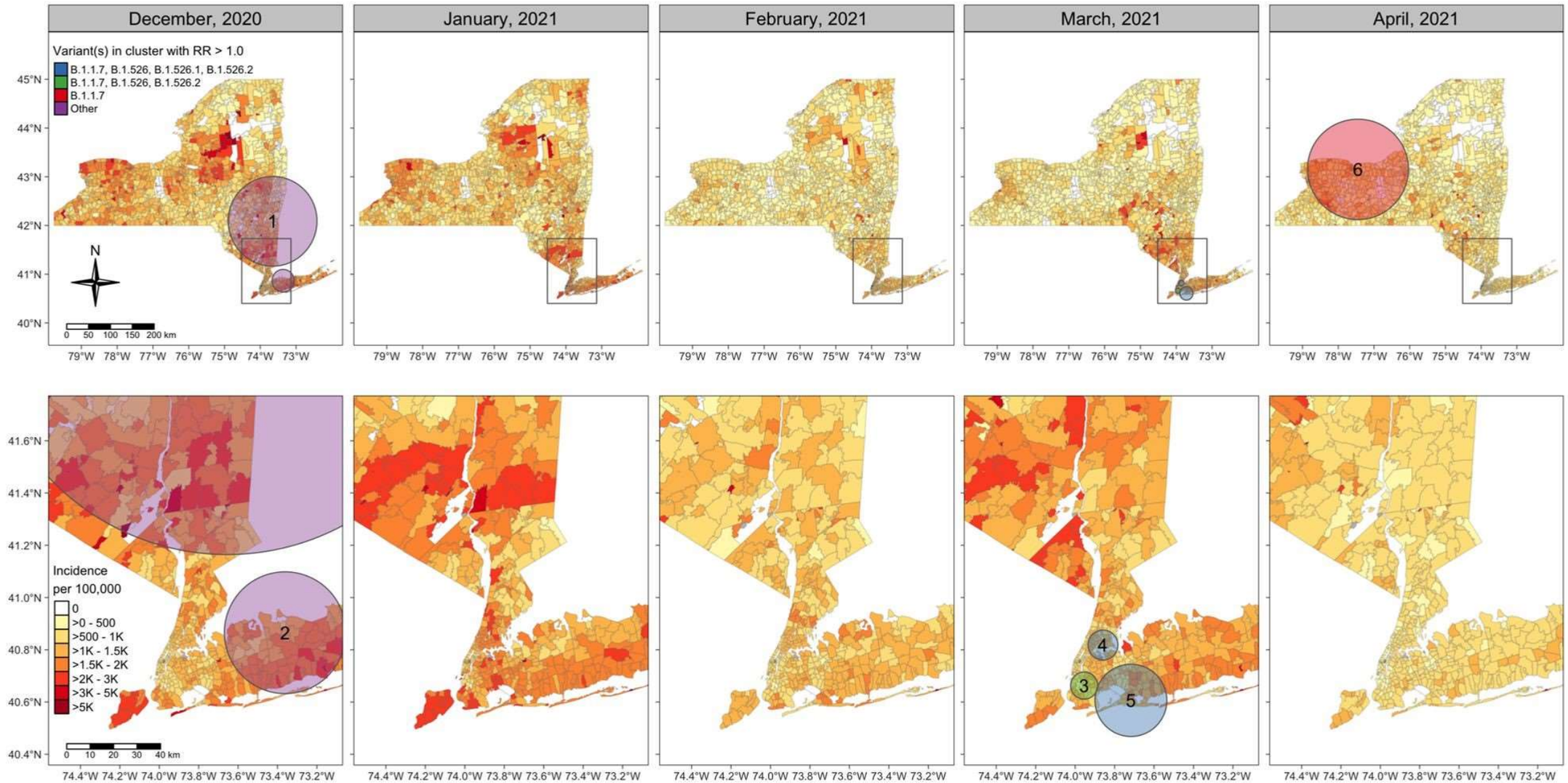
December, 2020
January, 2021
February, 2021
March, 2021
April, 2021
Variant(s) in cluster with RR > 1.0
B.1.1.7, B.1.526, B.1.526.1, B.1.526.2
B.1.1.7, B.1.526, B.1.526.2
B.1.1.7
Other
1
2
3
4
5
6
N
0 50 100 150 200 km
0 10 20 30 40 km
Incidence per 100,000
0
>0 - 500
>500 - 1K
>1K - 1.5K
>1.5K - 2K
>2K - 3K
>3K - 5K
>5K
45°N
44°N
43°N
42°N
41°N
40°N
41.6°N
41.4°N
41.2°N
41.0°N
40.8°N
40.6°N
40.4°N
79°W 78°W 77°W 76°W 75°W 74°W 73°W
74.4°W 74.2°W 74.0°W 73.8°W 73.6°W 73.4°W 73.2°W

Figure 4A

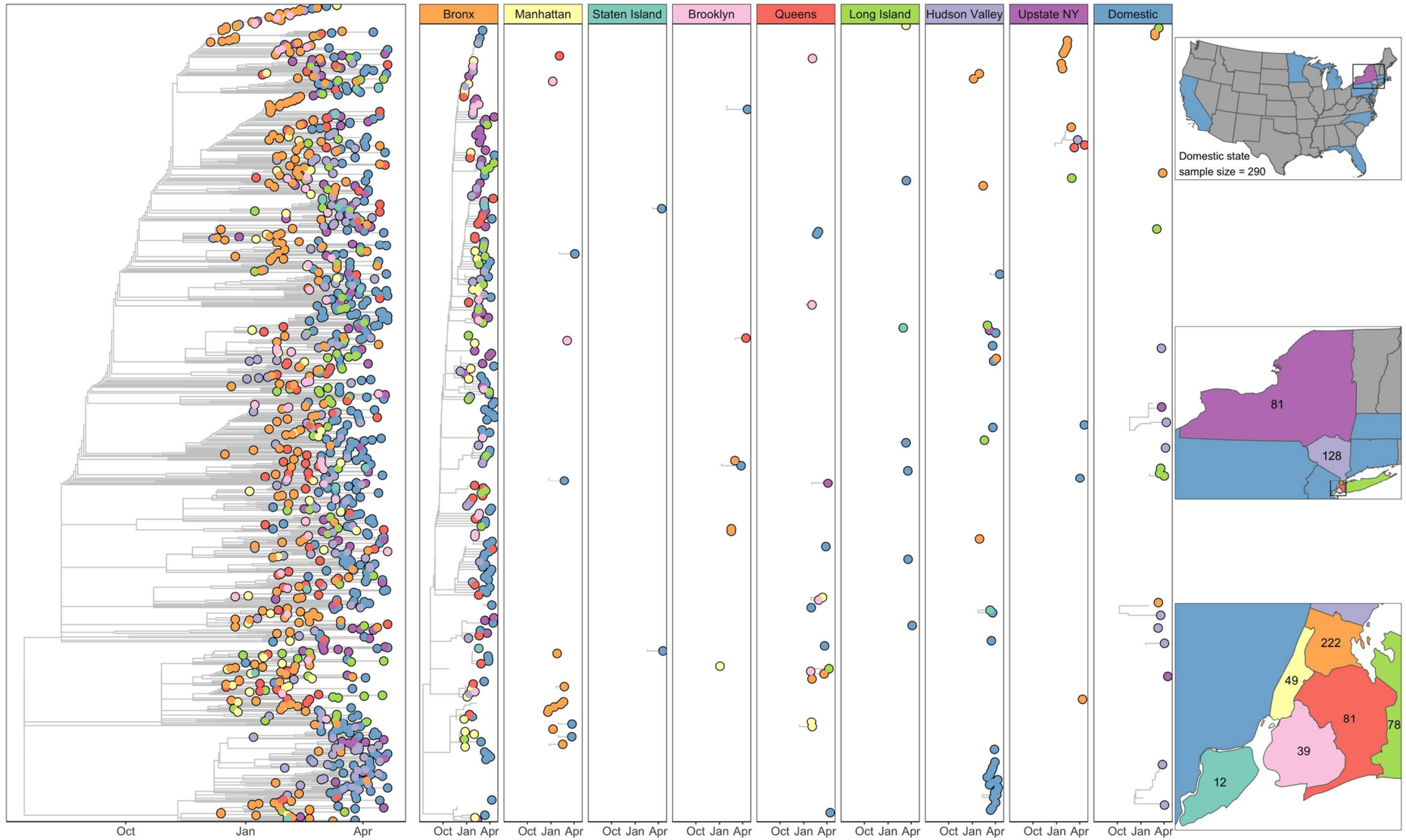
Bronx
Manhattan
Staten Island
Brooklyn
Queens
Long Island
Hudson Valley
Upstate NY
Domestic
Oct
Jan
Apr
Domestic state
sample size = 290
81
128
222
49
81
78
39
12

Figure 4B

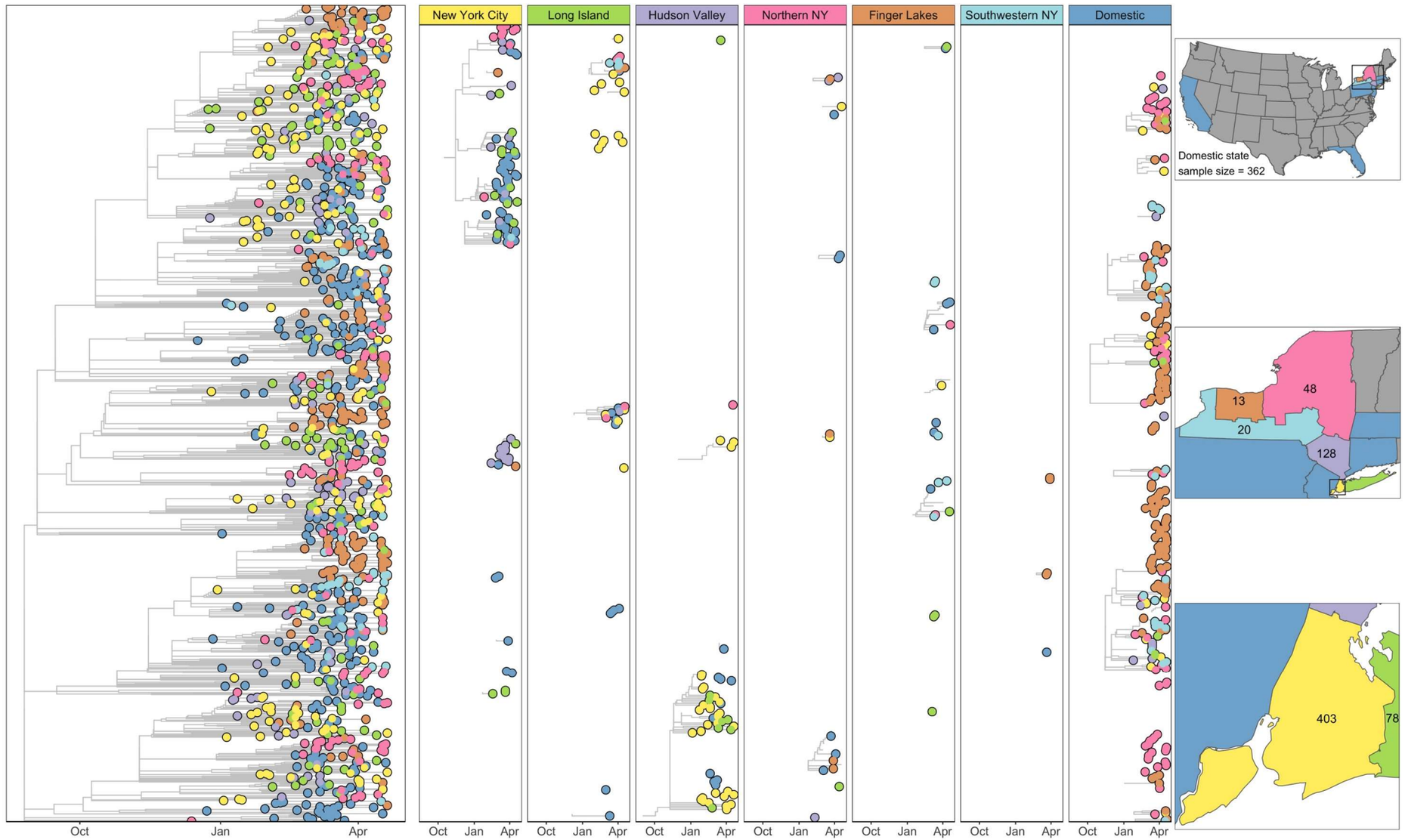
New York City
Long Island
Hudson Valley
Northern NY
Finger Lakes
Southwestern NY
Domestic
Oct
Jan
Apr
Domestic state
sample size = 362
48
13
20
128
403
78